Reconfigurable cavity-based plasmonic platform for resonantly enhanced sub-bandgap photodetection F

Cillian P. T. McPolin, Mayela Romero-Gómez, Alexey V. Krasavin, Wayne Dickson, and Anatoly V. Zayats

COLLECTIONS

Paper published as part of the special topic on Hot Electron Physics and Applications

F   This paper was selected as Featured

View Online   Export Citation   CrossMark

ARTICLES YOU MAY BE INTERESTED IN

Hybrid organic–inorganic halide perovskites
Journal of Applied Physics **128**, 200401 (2020); https://doi.org/10.1063/5.0034825

Hot-carrier enhanced light emission: The origin of above-threshold photons from electrically driven plasmonic tunnel junctions
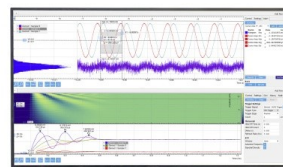Journal of Applied Physics **128**, 233105 (2020); https://doi.org/10.1063/5.0024392

Reactive fluxes delivered by plasma jets to conductive dielectric surfaces during multiple reflections of ionization waves
Journal of Applied Physics **128**, 203301 (2020); https://doi.org/10.1063/5.0019350

Reconfigurable cavity-based plasmonic platform for resonantly enhanced sub-bandgap photodetection Ⓕ

Cillian P. T. McPolin,[a)] Ⓘ Mayela Romero-Gómez, Ⓘ Alexey V. Krasavin, Wayne Dickson, Ⓘ and Anatoly V. Zayats[a)] Ⓘ

AFFILIATIONS

Department of Physics and London Centre for Nanotechnology, King's College London, Strand, London WC2R 2LS, United Kingdom

Note: This paper is part of the Special Topic on Hot Electron Physics and Applications.
[a)]**Authors to whom correspondence should be addressed:** cillian.mcpolin@kcl.ac.uk and a.zayats@kcl.ac.uk

ABSTRACT

Sub-bandgap photodetection based on plasmonic excitations represents a promising route for expanding the spectral range of photodetectors, enabling, for instance, silicon-based devices to be employed at telecom wavelengths. This approach harnesses internal photoemission, where hot carriers are generated via nonradiative plasmonic decay and are subsequently emitted from the metal to a semiconductor, yielding a photocurrent not spectrally limited by the bandgap. However, many schemes based on this approach suffer from low responsivities that hinder their uptake in real-world technologies. Here, we demonstrate a cavity-based platform for both enhancing the generated photocurrent and providing a means for dynamic reconfiguration of the operating wavelength. The proposed device is composed of an optical cavity where one of the mirrors is patterned with a nanoscale grating and interfaced at the other side with a semiconductor. Fabry–Pérot resonances supported by the cavity provide resonant excitation of plasmonic modes at the metal/semiconductor interface, leading to augmented hot-carriers and photocurrent generation compared to the non-resonant case. By employing this cavity-grating geometry, we experimentally demonstrate a fivefold increase in photocurrent due to the presence of cavity resonances. Electromechanical reconfiguration of the photodetector cavity length is also achieved, illustrating dynamic control over the detection wavelength. This cavity-based architecture is compatible with a variety of plasmonic nanostructures, including nanoparticles and nanoantennas, thus providing a flexible means of significantly increasing the photoresponse and hence bringing on-chip plasmonic hot-carrier technologies closer to realization for sub-bandgap photodetection, energy harvesting, and sensing.

I. INTRODUCTION

The ability to efficiently convert light into electricity is essential for many applications, not least for photodetection and solar energy harvesting. This is typically achieved by using absorption in semiconductors, where, upon absorption, photons that match, or exceed, the semiconductor bandgap generate electron–hole pairs that are subsequently separated, giving rise to a photocurrent. However, photons with energies below the bandgap energy cannot excite electron–hole pairs and, therefore, cannot be detected. Consequently, semiconductors cannot be employed in efficient photodetectors at wavelengths below their bandgap, which, in the case of silicon, represents a major hurdle in the realization of many integrated silicon-based technologies, for instance, in optical communications. Effectively expanding the spectral range of silicon further into the infrared, encompassing telecom wavelengths

(1.3–1.6 μm), would herald a new era in silicon photonics, circumventing the need for costly materials that are complex to fabricate and not CMOS compatible (e.g., III–V semiconductors).[1] To this end, the bandgap limit can be overcome by interfacing silicon with a metal, resulting in the formation of a Schottky barrier, where optical absorption occurs in the metal itself and the generated hot carriers (hot electrons or holes) are subsequently emitted over the barrier into the adjacent semiconductor, the so-called internal photoemission (IPE)[2–4] process. This yields a photocurrent via the flow of either hot electrons or hot holes, which are inhibited from recombining, making a photodetector utilizing a Schottky barrier a majority carrier device. Photodetection is, therefore, dictated by the height of the metal–semiconductor Schottky barrier, rather than the semiconductor's bandgap, enabling the detection of sub-bandgap photons. Moreover, the Schottky barrier height for a

p-type silicon–gold interface has been previously reported as ~0.32 eV,[5] and thus such a configuration allows for silicon-based detectors to effectively operate much further into the infrared, at energies below the bandgap of ~1.1 eV. This IPE-based method fundamentally relies on photon absorption and hot-carrier generation, which in unstructured metals is typically not efficient as light is strongly reflected. However, by harnessing surface plasmon excitations that arise due to the coupling of light to electron oscillations in the metal,[6] one can significantly increase absorption in nanostructures.[7] The nonradiative decay of these plasmonic excitations gives rise to hot carriers (electron–hole pairs), making them an ideal means of producing a sub-bandgap photocurrent. Moreover, as plasmonic modes are localized at the surface of the metal structure, the hot carriers they produce are also naturally near the surface and, therefore, can be readily harnessed in an adjacent medium, not only for photodetection but also for catalysis[8] and photochemical transformations.[9,10] Consequently, hot-carrier plasmonics is becoming a rapidly growing field, offering opportunities for a wide range of applications, including sensing and energy harvesting.[11–14] Successfully combining silicon photonics with plasmonics may enable on-chip silicon-based infrared photodetectors for a whole host of technologies.[15]

The promise of this approach is evidenced by the wide variety of schemes recently proposed for plasmonic-enhanced sub-bandgap photodetection, which can be loosely grouped into waveguides,[16–18] gratings,[19] nanoparticles,[20] nanoantennas,[21–23] pyramids,[24,25] metamaterials,[26] arrays of nanostructures,[27] and self-organized films,[28] where the photocurrent originates from propagating and/or localized plasmonic modes. Many studies have also addressed in detail the physics of hot-carrier generation, transport, and emission occurring in such plasmonic systems, and which also confirm the significant potential of this nanostructured metal-based approach.[7,29,30] In terms of materials, gold has been shown to facilitate significant photocurrents, while alternative materials, such as titanium nitride,[31] are also being explored, in addition to hybrid graphene schemes.[32] However, tunable photodetection schemes, in which the detection wavelength can be dynamically altered, have not been exploited to date. Such reconfigurable architectures would provide new opportunities for spectroscopy and polarimetry, and thus it is essential to develop new approaches for their realization.[33]

In this context, here we have developed a resonantly enhanced photodetector that concurrently provides both augmented sub-bandgap photoresponse and spectral tunability, thus fulfilling key requirements for the next generation of silicon-based integrated infrared photodetectors.[34] Our approach is based on a straightforward gold cavity-grating configuration for a proof-of-principle experiment that can be easily iterated upon (with regard to materials and geometry) to address all the considerations for an optimized sub-bandgap photodetector and can be applied as a universal enhancement approach for various plasmon-based photodetector architectures.

II. DESIGN CONCEPT

The proposed geometry is shown in Fig. 1(a)—an optical cavity is formed between two gold mirrors. One of the mirrors is nanostructured in the form of a grating that resonantly couples the
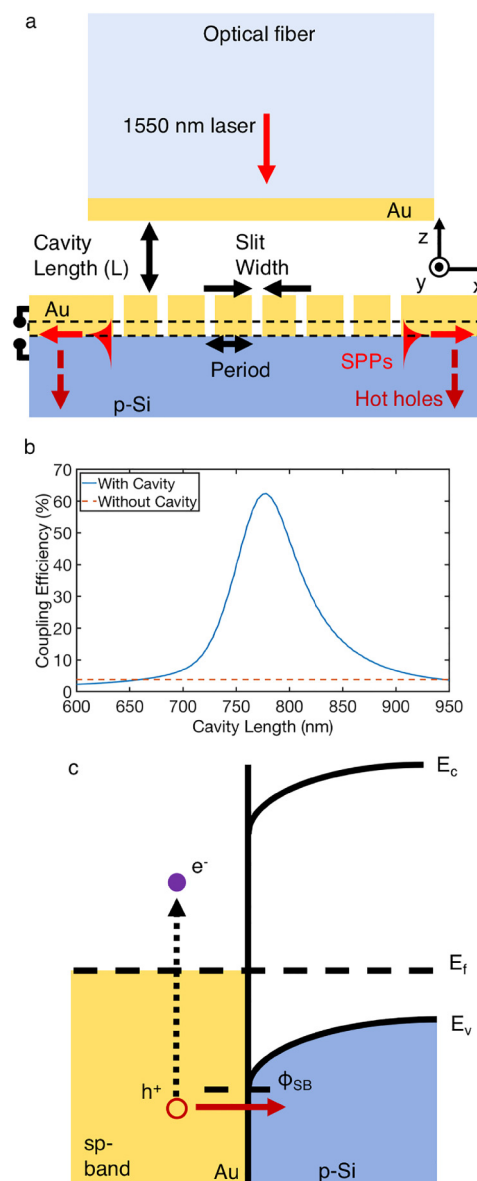
FIG. 1. Resonantly enhanced plasmonic photodetector. (a) Geometry of the cavity-based photodetector. The gold-coated fiber simultaneously provides illumination of the grating and also forms the upper mirror of the cavity, resulting in optical resonances for specific cavity lengths. The efficiency of the SPP generation is resonantly enhanced at the Au/p-Si interface when a cavity mode is sustained between the two gold films, yielding a significantly increased photocurrent. (b) Calculated Au/Si SPP coupling efficiency for illumination of the grating via a gold-coated fiber as the cavity length is varied. Coupling efficiency for grating without a cavity is shown by the red dashed line. Coupling efficiency is defined as the ratio between the SPP power and the power of the illuminating light: (solid blue line) exiting the gold-coated fiber in the cavity case and (dashed red line) a free space beam incident on the grating. (c) Energy band diagram of the Schottky junction formed between gold and p-type silicon. Hot holes are injected over the Schottky barrier, giving rise to a photocurrent. E_f is the Fermi energy, E_v is the top of the valence band, and E_c is the bottom of the conduction band.

excited cavity modes to surface plasmon polaritons (SPPs) at the metal-semiconductor interface.[35] These SPPs subsequently decay, producing hot carriers that give rise to a photocurrent. Thus, by actively controlling the resonance conditions via the change of the cavity length, we can directly modify the wavelength of the resonant SPP generation and hence the peak photodetection wavelength. In this case, a grating is employed to excite SPPs via photon momentum matching with quite a large bandwidth (due to its few-period realization). Such periodic structures have been previously used to enable photocurrent generation[19,36–38] and are also amenable to on-chip integration.[39]

A Monte Carlo optimization process was used in order to numerically determine the optimal grating parameters for the SPP generation and thus photodetection around a wavelength of 1550 nm, which involved maximizing the absorption in a 20 nm thick region of the gold film at the silicon interface, i.e., maximize SPP excitation and thus hot-carrier generation, at the Au/Si interface. The SPP penetration depth into the Au film is ∼20 nm at 1550 nm incident free space wavelength, comparable to the typical mean free paths of hot carriers, as indicated in Fig. 1(a). This yielded the following geometric parameters: 80 nm slit width, 300 nm gold thickness, and 1240 nm grating period. The slit length was fixed at $15\,\mu m$, with 10 slits forming the grating. It is important to note that increasing the number of slits, apart from narrowing its operational bandwidth, may lead to higher radiative losses and hence lower photoresponse. Illumination of the grating structure via a gold-coated optical fiber mounted on a piezoelectric stage allows for the cavity length to be directly varied, thus controlling the spectral position of the Fabry–Pérot cavity modes. The gold film covering the fiber was 10 nm thick, which facilitates cavity modes while also ensuring low absorption in the upper mirror. The light coupling efficiency to the Au/Si SPP is estimated from the simulations to be ∼60% when the cavity is on the first resonance, which is considerably greater compared to 4% efficiency obtained when the cavity is absent [Fig. 1(b)]. This resonant increase of the coupling efficiency is also in good agreement with the previous studies of cavity-enhanced SPP excitation.[35]

P-type silicon was used as a semiconducting contact such that hot holes are injected from the gold into the silicon over the Schottky barrier [Fig. 1(c)], which can potentially provide higher currents than in the case of n-type silicon.[5] As the illumination wavelength of 1550 nm is far from the interband transition threshold in gold (∼2.2 eV), there are effectively no holes generated in the d-band via direct, d–sp transitions. Upon absorption of the electromagnetic energy, the hot holes may originate from indirect, intraband transitions in the sp-band, facilitated by the field enhancement associated with the SPPs and the required momentum conservation provided by the scattering by phonons and/or interfaces and roughness of the device geometry, or the decay of a SPP producing an electron–hole pair.[40,41] In order to fully optimize the induced photocurrent, the hot-carrier generation, transport, and injection must be carefully considered in terms of the barrier height and the mean free path, together with the energy and momentum distributions of the excited hot carriers. Nanoscale features at the metal/semiconductor interface are beneficial for providing momentum relaxation of the carriers and their transfer to the semiconductor.[42]

III. EXPERIMENT AND SIMULATION METHODS

In the experiments, the lower mirror of the cavity was formed from a 300 nm gold film that was deposited on p-type silicon with a 2 nm titanium adhesion layer. Both Au and Ti layers were produced by DC magnetron sputter deposition on a single side polished p-type Si wafer (⟨100⟩ orientation, Boron dopant, resistivity 1–10 Ω-cm), which was previously etched in a 10% HF solution for the removal of the native SiO_2 layer. The gratings were subsequently focused ion beam milled into this film. The upper mirror was produced from a cleaved surface of a polarization maintaining fiber by coating it with a 10 nm thin Au layer, via thermal evaporation. A tunable infrared laser coupled to the fiber, with or without
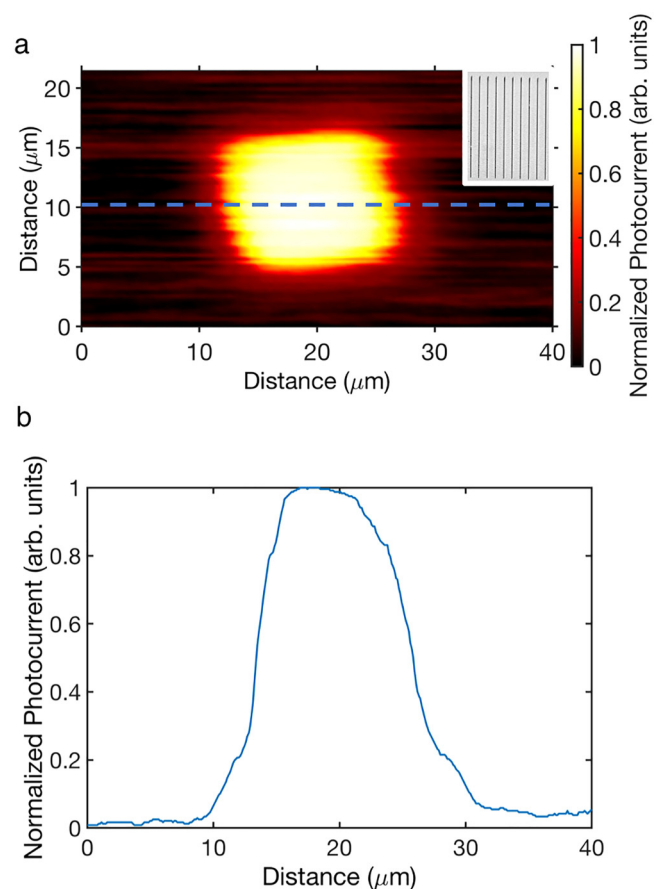
FIG. 2. Mapping photocurrent from a grating device without a cavity. (a) Photocurrent map obtained when illuminating the grating region through a raster-scanned cleaved fiber at a wavelength of 1550 nm. The illuminating light is linearly polarized with the electric field perpendicular to the grating slits. The typical measured dark current was ∼10 nA at zero bias, as devices based on p-type silicon exhibit greater noise due to the lower Schottky barrier. Inset: Scanning electron microscopy image of the grating used in (a) with a slit width of 80 nm, a period of 1240 nm, and a slit length of $15\,\mu m$. (b) A cross section of the photocurrent map as indicated in (a), illustrating the photoresponse coinciding with the position of the grating. Photocurrent has been normalized to 1 in (a) and (b).

the gold mirror, was used as a light source for the experiments with or without a cavity, respectively. The fiber was mounted on a piezoelectric positioner, permitting nanometric x–y–z control. Photoresponsivity was measured with respect to the optical power leaving the gold-coated optical fiber. A finite element method (COMSOL Multiphysics 4.3a) was employed to model the cavity-grating system.

IV. RESULTS AND DISCUSSION

Initially, the photocurrent was mapped from an isolated grating (i.e., without a cavity), in order to confirm the plasmonic origin of the response. The output from an uncoated cleaved fiber was scanned across the surface of the grating, with the resulting current recorded for each position [Fig. 2(a)]. A clear hotspot, with a size closely matching that of the milled grating, is evident in the current map, with a cross section shown in Fig. 2(b). Moreover, no appreciable photocurrent was observed when the incident beam was polarized parallel to the slits or when the gold film is directly illuminated, confirming the plasmonic nature of the hotspot. It is important to note that as the gold thickness is 300 nm, only the SPPs at the Si interface will effectively contribute to the photocurrent, as the mean free path of hot holes is on the order of 10s of nanometers in gold,[5] so any holes that are generated near the top interface (via direct absorption or plasmonic decay) will lose energy via scattering before reaching the silicon interface; as a result, their energy will be below the Schottky barrier height and thus they cannot contribute to the photocurrent. Conversely, SPPs that propagate at the Au/Si interface generate hot holes in the region directly adjacent to the silicon substrate, thereby ensuring a high probability of their transfer into the semiconductor.

Once SPP-induced photocurrent was demonstrated, the second mirror, formed from the cleaved fiber coated with a 10 nm thin Au film, was placed above the grating and scanned in the z-direction in order to elucidate the influence of the optical cavity modes. The spectral response of the cavity-grating photodetector is shown in Fig. 3(a), where the incident wavelength varied from 1500 to 1580 nm. The role of the Fabry–Pérot modes is clearly apparent, providing much greater photocurrent in the resonant conditions than off resonance, due to resonant scattering from the grating and thus resonant excitation of the substrate (Au/Si) SPPs. Here, the cavity mode wavelength is given by $\lambda = 2L/N$, where L is the cavity length and N the integer mode number. The bright band for all cavity lengths in the range ~1540–1560 nm is most likely a consequence of the grating being more efficient in generating SPPs in this range as it was designed to provide a maximum substrate plasmonic coupling efficiency at 1550 nm.

The proposed approach also enables direct control over the detection wavelength, as the resonance conditions can be dynamically tuned. This is highlighted in Fig. 3(a), as the peak response is electromechanically tuned over the spectral range of the laser by altering the z-position of the top mirror and, therefore, the cavity length. The high photocurrent stability, which is crucial for practical applications, is also observed in Fig. 3(b), as the cavity is scanned back and forth through a cavity resonance. Here, the response is symmetric about the 50 s mark and stable over the complete period of 100 s.

The photocurrent from this resonant system reaches over ~5 μA/W, an approximately five times increase compared to the off resonance condition (e.g., comparing the photocurrents at 28 s and 50 s), as illustrated in Fig. 3(b). While the absolute value of the measured photocurrent is modest (which may be due to the
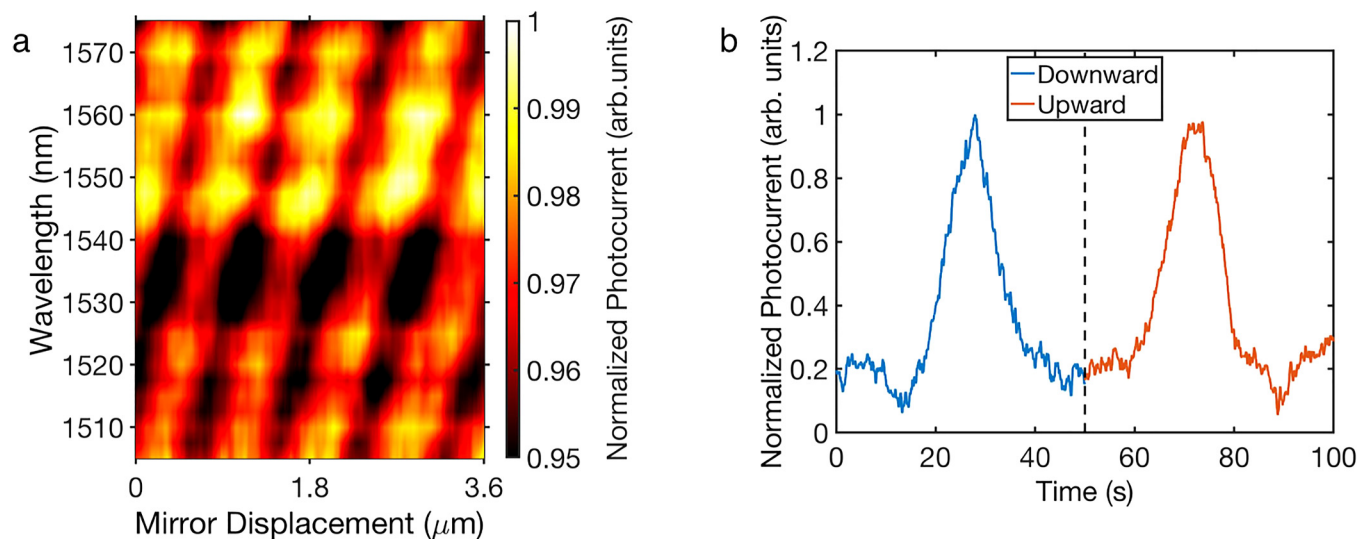

FIG. 3. Resonantly enhanced photodetection. (a) Spectral dependence of the photocurrent as the cavity length is varied, illustrating the role of the cavity modes. (b) The dependence of the photocurrent on the cavity length: the top mirror is moved downward and upward over a time period of 100 s, scanning one of the Fabry–Pérot modes at a fixed wavelength of 1550 nm. At t = 0 s and t = 100 s, the fiber is at its highest point and at t = 50 s, the fiber is positioned at its lowest point. Blue and red portions of the scan indicate the fiber moving downward and upward, respectively. Photocurrent has been normalized to 1 in (a) and (b).

absence of the roughness at the Au/Si interface needed to promote efficient carrier transfer from Au to Si), the key advantage is the observed enhancement over the baseline current, as it offers a straightforward means to augment the performance of a wide range of plasmonic-based photodetectors. The lower mirror could be composed of an array of nanoparticles on a silicon substrate coated in a thin metal film, as small nanoparticles provide more efficient hot-carrier generation and injection via the geometry-assisted electron scattering mechanism.[40,43] The highest photoresponsivities of hot-carrier mediated plasmonic-silicon photodetectors reported to date at a wavelength of 1550 nm are of the order of hundreds of μA/W at zero bias achieved with trench and grating antennas,[21,19] nanoantennas,[22] and nanopyramids.[25] Our cavity-based scheme is compatible with these architectures and hence has the potential to further increase their performance. We also note that while a degree of surface roughness is advantageous on the Au/Si interface, as it could aid in the injection of hot carriers to the silicon via relaxing the hot-carrier momentum mismatch,[42,44] it is deleterious on the upper grating surface (Au/air interface) as it will reduce the cavity Q-factor.

In order to demonstrate reconfigurability and spectral tuneability, the cavity length in the presented experiments was on the order of tens of micrometers. Much smaller cavities can be explored based on a solid-state layered system optimized to provide the enhancement at a fixed wavelength in compact devices for on-chip integration. It has been previously shown that such a cavity configuration can be actively tuned via all-optical and electrical means,[35] further expanding the opportunities for the device applications. For instance, in one embodiment, the device can be configured as a pressure sensor, as the position of the upper mirror directly impacts the current generated.

By using cavity resonances, we are able to achieve narrowband detection, which is critical for wavelength-sensitive applications.[45] Effectively, the cavity structure serves as a means to efficiently excite SPPs at the Au/Si interface to achieve significant generation of hot carriers in the gold film adjacent to the silicon layer. The underlying mechanism of this resonant enhancement is further clarified via numerical simulations presented in Fig. 4. When the cavity is on resonance [L = 775 nm, Fig. 4(a) right panel], a clear enhancement is observed in the intensity of Au/Si SPPs, due to resonant scattering from the grating, when compared to the non-resonant case [L = 610 nm, Fig. 4(a) left panel], with negligible excitation of parasitic Au/air SPPs in both cases. This leads to metal absorption at the Au/Si interface that is approximately ten times greater than in the non-resonant case. It is also approximately six times greater compared to the absorption at the superstrate interface when on resonance [Fig. 4(b)]. In addition, the device exhibits a narrowband response [Fig. 4(c)], which illustrates the spectral dependence of the absorption in the Au film near the Si/Au interface at a fixed cavity length of 775 nm. The absorption peaks at 1550 nm with the FWHM ~50 nm, thus potentially offering a narrower response compared to previous works employing isolated gratings,[19] which is particularly advantageous for wavelength-selective applications. Interestingly, the absorption in the upper metal film has an asymmetric line shape, which aids in minimizing the loss associated with direct absorption in this region when on resonance. This effect also occurs in the absence of the
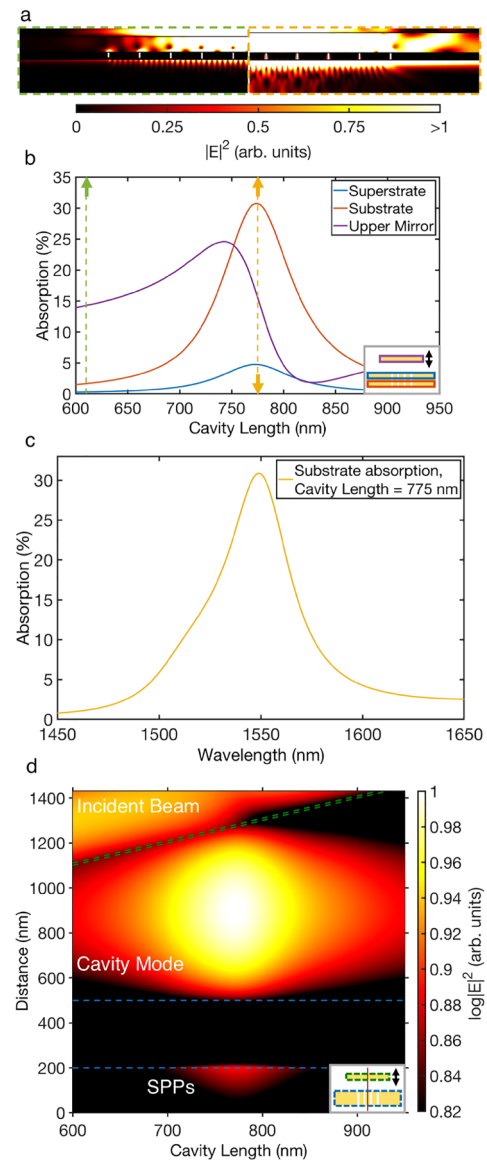
FIG. 4. Simulations of the cavity-enhanced photodetection at a wavelength of 1550 nm. (a) Electric field distribution ($|E|^2$) for the photodetector off (left panel, green dashed line, 610 nm cavity length) and on (right panel, orange dashed line, 775 nm cavity length) resonance, indicating the Au/Si SPP enhancement in the presence of a cavity mode. (b) Absorption in the different regions of the device as the cavity length is varied (upper mirror displaced): absorption near an air superstrate (blue line) and Si substrate (red line) was calculated in 20 nm thin regions within the lower Au film adjacent to the Au/Air and Au/Si interfaces, respectively. The upper mirror absorption (purple line) is also presented. Dashed green and orange lines correspond to the cavity lengths shown in (a). (c) Spectral dependence of the absorption in the Au film near the Si/Au interface at a fixed cavity length of 775 nm. (d) Electric field distribution (log $|E|^2$) sampled along a line in the z-direction through the center of the structure as the cavity length is varied. Dashed green and blue lines indicate the positions of the interfaces of the upper and lower Au films. The regions predominantly containing incident beam, cavity mode, and Au/Si SPPs are also marked.

grating and can be understood in terms of the electric field localization [Fig. 4(d)]. Here, the electric field was evaluated along a line in the z-direction as the upper mirror is moved through the resonance. The hotspot below the lower Au mirror directly corresponds to the resonantly excited substrate SPPs, which is absent when the beam is polarized parallel to the slits. As the cavity moves through the N = 1 Fabry–Pérot mode, the field within upper mirror increases, before sharply decreasing, giving rise to the distinctive asymmetric absorption line shape due to Fabry–Pérot interference. Conversely, the symmetric line shapes exhibited by the lower mirror [both the substrate and superstate, Fig. 4(b)] are indicative of solely resonant absorption. Furthermore, controlling the absorption in lossy, thin metal films is an increasingly active area of research, and thus this cavity system may also provide opportunities for developing new approaches for, e.g., color filters[46,47] or wavelength-selective photodetector arrays.[48]

V. CONCLUSION

We have successfully performed a proof-of-principle experiment illustrating the resonantly enhanced and wavelength-tunable photoresponse of sub-bandgap detectors afforded by a cavity-based architecture. The device exploits resonantly driven plasmonic modes to significantly improve the performance of sub-bandgap photodetectors. A fivefold increase in the photocurrent was recorded compared to the non-resonant case, illustrating the potential of this cavity-based approach which can be adapted to include other plasmonic nanostructures for even greater responsivity. Moreover, we have also demonstrated dynamic tunability with respect to the operating wavelength, thereby expanding the functionality of the developed technology and paving the way for future reconfigurable photodetectors for wavelength-selective applications.

ACKNOWLEDGMENTS

DATA AVAILABILTY

The data that support the findings of this study are available from the corresponding author upon reasonable request.

REFERENCES

[1]M. Casalino, G. Coppola, R. M. De La Rue, and D. F. Logan, Laser Photonics Rev. 10, 895 (2016).
[2]J. Tong, F. Suo, J. Ma, L. Y. M. Tobing, L. Qian, and D. H. Zhang, Opto-Electron. Adv. 2, 180026 (2019).
[3]A. Dorodnyy, Y. Salamin, P. Ma, J. Vukajlovic Plestina, N. Lassaline, D. Mikulik, P. Romero-Gomez, A. Fontcuberta i Morral, and J. Leuthold, IEEE J. Sel. Top. Quantum Electron. 24, 1 (2018).
[4]W. Li and J. G. Valentine, Nanophotonics 6, 177 (2017).
[5]Q. Sun, C. Zhang, W. Shao, and X. Li, ACS Omega 4, 6020 (2019).
[6]A. V. Zayats, I. I. Smolyaninov, and A. A. Maradudin, Phys. Rep. 408, 131 (2005).

[7]B. Y. Zheng, H. Zhao, A. Manjavacas, M. McClain, P. Nordlander, and N. J. Halas, Nat. Commun. 6, 7797 (2015).
[8]J. U. Salmon-Gamboa, M. Romero-Gomez, D. J. Roth, M. J. Barber, P. Wang, S. M. Fairclough, M. E. Nasir, A. V. Krasavin, W. Dickson, and A. V. Zayats, Faraday Discuss. 214, 387 (2019).
[9]M. L. Brongersma, N. J. Halas, and P. Nordlander, Nat. Nanotechnol. 10, 25 (2015).
[10]P. Wang, A. V. Krasavin, M. E. Nasir, W. Dickson, and A. V. Zayats, Nat. Nanotechnol. 13, 159 (2018).
[11]A. V. Zayats and S. Maier, Adv. Opt. Mater. 5, 1700508 (2017).
[12]M. L. Brongersma, Proc. IEEE 104, 2349 (2016).
[13]H. Tang, C. J. Chen, Z. Huang, J. Bright, G. Meng, R. S. Liu, and N. Wu, J. Chem. Phys. 152, 220901 (2020).
[14]H. Reddy, K. Wang, Z. Kudyshev, L. Zhu, S. Yan, A. Vezzoli, S. J. Higgins, V. Gavini, A. Boltasseva, P. Reddy, V. M. Shalaev, and E. Meyhofer, Science 369, 423 (2020).
[15]B. Feng, J. Zhu, B. Lu, F. Liu, L. Zhou, and Y. Chen, ACS Nano 13, 8433 (2019).
[16]Y. Su, C. Lin, P. Chang, and A. S. Helmy, Optica 4, 1259 (2017).
[17]I. Goykhman, B. Desiatov, J. Khurgin, J. Shappir, and U. Levy, Opt. Express 20, 28594 (2012).
[18]A. Akbari and P. Berini, Appl. Phys. Lett. 95, 021104 (2009).
[19]A. Sobhani, M. W. Knight, Y. Wang, B. Zheng, N. S. King, L. V. Brown, Z. Fang, P. Nordlander, and N. J. Halas, Nat. Commun. 4, 1643 (2013).
[20]Z. Qi, Y. Zhai, L. Wen, Q. Wang, Q. Chen, S. Iqbal, G. Chen, J. Xu, and Y. Tu, Nanotechnology 28, 275202 (2017).
[21]K. T. Lin, C. J. Chan, Y. S. Lai, L. T. Shiu, C. C. Lin, and H. L. Chen, ACS Appl. Mater. Interfaces 11, 3150 (2019).
[22]K. T. Lin, H. L. Chen, Y. S. Lai, and C. C. Yu, Nat. Commun. 5, 3288 (2014).
[23]M. W. Knight, H. Sobhani, P. Nordlander, and N. J. Halas, Science 332, 702 (2011).
[24]B. Desiatov, I. Goykhman, N. Mazurski, J. Shappir, J. B. Khurgin, and U. Levy, Optica 2, 335 (2015).
[25]Y. Zhai, Y. Li, J. Ji, Z. Wu, and Q. Wang, ACS Appl. Nano Mater. 3, 149 (2020).
[26]W. Li and J. Valentine, Nano Lett. 14, 3510 (2014).
[27]Z. Yang, M. Liu, S. Liang, W. Zhang, T. Mei, D. Zhang, and S. J. Chua, Opt. Express 25, 20268 (2017).
[28]C. Frydendahl, M. Grajower, J. Bar-David, R. Zektzer, N. Mazurski, J. Shappir, and U. Levy, Optica 7, 371 (2020).
[29]G. Tagliabue, A. S. Jermyn, R. Sundararaman, A. J. Welch, J. S. DuChene, R. Pala, A. R. Davoyan, P. Narang, and H. A. Atwater, Nat. Commun. 9, 3394 (2018).
[30]R. Sundararaman, P. Narang, A. S. Jermyn, W. A. Goddard III, and H. A. Atwater, Nat. Commun. 5, 5788 (2014).
[31]J. Gosciniak, F. B. Atar, B. Corbett, and M. Rasras, Sci. Rep. 9, 6048 (2019).
[32]I. Goykhman, U. Sassi, B. Desiatov, N. Mazurski, S. Milana, D. de Fazio, A. Eiden, J. Khurgin, J. Shappir, U. Levy, and A. C. Ferrari, Nano Lett. 16, 3005 (2016).
[33]M. Oshita, H. Takahashi, Y. Ajiki, and T. Kan, ACS Photonics 7, 673 (2020).
[34]I. Goykhman, B. Desiatov, J. Khurgin, J. Shappir, and U. Levy, Nano Lett. 11, 2219 (2011).
[35]C. P. T. McPolin, N. Olivier, J. S. Bouillard, D. O'Connor, A. V. Krasavin, W. Dickson, G. A. Wurtz, and A. V. Zayats, Light Sci. Appl. 6, e16237 (2017).
[36]M. Tanzid, A. Ahmadivand, R. Zhang, B. Cerjan, A. Sobhani, S. Yazdi, P. Nordlander, and N. J. Halas, ACS Photonics 5, 3472 (2018).
[37]A. Takeda, T. Aihara, M. Fukuhara, Y. Ishii, and M. Fukuda, J. Appl. Phys. 116, 084313 (2014).
[38]M. Alavirad, A. Olivieri, L. Roy, and P. Berini, Opt. Express 24, 22544 (2016).
[39]C. P. T. McPolin, J.-S. Bouillard, S. Vilain, A. V. Krasavin, W. Dickson, D. O'Connor, G. Wurtz, J. Justice, B. Corbett, and A. V. Zayats, Nat. Commun. 7, 12409 (2016).

[40]A. M. Brown, R. Sundararaman, P. Narang, W. A. Goddard III, and H. A. Atwater, ACS Nano **10**, 957 (2016).

[41]G. Tagliabue, J. S. DuChene, A. Habib, R. Sundararaman, and H. A. Atwater, ACS Nano **14**, 5788 (2020).

[42]A. V. Krasavin, P. Wang, M. E. Nasir, Y. Jiang, and A. V. Zayats, Nanophotonics **9**, 427 (2020).

[43]Y. Liu, Q. Chen, D. A. Cullen, Z. Xie, and T. Lian, Nano Lett. **20**, 4322 (2020).

[44]M. Grajower, U. Levy, and J. B. Khurgin, ACS Photonics **5**, 4030 (2018).

[45]H. Xiao, S.-C. Lo, Y.-H. Tai, Y.-L. Ho, J. K. Clark, P.-K. Wei, and J.-J. Delaunay, Appl. Phys. Lett. **116**, 161103 (2020).

[46]H. Kocer, S. Butun, Z. Li, and K. Aydin, Sci. Rep. **5**, 8157 (2015).

[47]M. A. Kats and F. Capasso, Laser Photonics Rev. **10**, 735 (2016).

[48]Z. Yang, T. Albrow-Owen, H. Cui, J. Alexander-Webber, F. Gu, X. Wang, T.-C. Wu, M. Zhuge, C. Williams, P. Wang, A. V. Zayats, W. Cai, L. Dai, S. Hofmann, M. Overend, L. Tong, Q. Yang, Z. Sun, and T. Hasan, Science **365**, 1017 (2019).